

## TAILORING OXYGEN DISTRIBUTION IN 300MM CZOCHRALSKI CRYSTAL OF PURE SILICON USING CUSP MAGNETIC FIELD

**Prashant GUNJAI<sup>1</sup> and Palghat RAMCHANDRAN**

<sup>1</sup> Department of Energy Environmental and Chemical Engineering,  
 Washington University in St. Louis, MO 63130, USA

### ABSTRACT

Oxygen content in the pure Silicon crystal is inevitable because of the significant rate of corrosion of the crucible walls at high temperature. Precise control of oxygen concentration in the crystal is possible only by manipulating underlying flow characteristics of the melt. Thermo-fluidics in this process are extremely complex and responsible for non-uniform oxygen striations. This work is focused to understand the melt flow complexities and its influence on oxygen distribution near the crystallization front. A global model which accounts for hardware configuration is considered for this purpose. The melt flow characteristics are investigated to study the effect of crystal and crucible rotations in absence and presence of the electromagnetic fields (EMs). Our simulation results show that strong buoyancy driven flow interaction generates non-uniformity in oxygen concentration near the edge of the crystal in the absence of magnetic field. Application of external field facilitates more pumping of melt underneath the crystal that prevents stratification of oxygen near the edge.

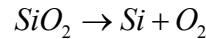
### NOMENCLATURE

<b>B</b>	Magnetic field intensity
$C_o$	oxygen concentration
$C_p$	heat capacity
$De$	Diffusion coefficient
$F_m$	Lorentz force
$g$	gravitation constant
$G_b$	generation of turbulent kinetic energy due to buoyancy
$G_k$	generation of turbulent kinetic energy
$j$	current density
$k$	turbulent kinetic energy, thermal conductivity
$kg$	mass transfer coefficient
$kt$	turbulent thermal conductivity
$L$	characteristic length
$P$	pressure
$r$	radial dimension
$T$	temperature
$v$	velocity vector
$z$	axial dimension
$\beta$	coefficient of thermal expansion
$\epsilon$	turbulent dissipation rate
$\mu_t$	turbulent kinematic viscosity
$\rho$	density

### INTRODUCTION

The Czochralski Growth (Cz) is extensively used for the manufacturing of single Silicon crystal. However, process control of this system is a crucial task for controlling quality of the crystal. Presence of oxygen in a grown crystal is one of the major factors for defects in the crystal or sometimes it is beneficial for controlling the crystal conductivity (Ramachandran et al., 1990). The materials used in producing semiconductor devices and microprocessors require precise control over the distribution of the oxygen in the crystals.

The schematic of overall transport of oxygen in Cz-Si process is shown in **Figure 1**. Presence of oxygen in the Si crystal is inevitable, since silica crucible dissolves into the molten Silicon and oxygen is transported into the melt from silica crucible through following reaction;



Melt carries most of the oxygen towards the gas-melt interface where it interact with the oxygen in the gas phase to form  $SiO(g)$ . Evaporation occurs at gas-melt interface and remaining oxygen gets incorporated into the crystal.

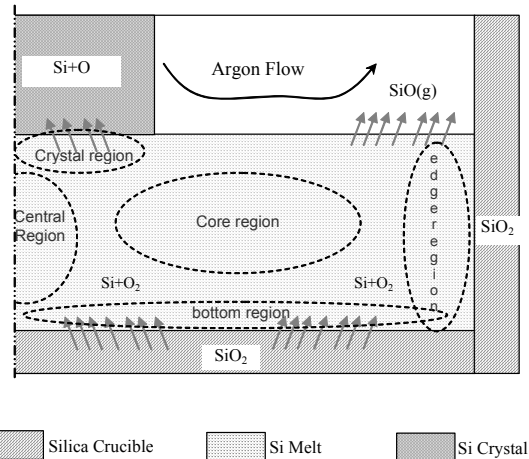


**Figure 1:** Schematic diagram of geometry

Oxygen concentration in the crystal is determined by the rate of dissolution of the silica crucible and the rate of evaporation of the oxygen in the form of  $SiO(g)$ . Rate of dissolution of the silica is a function of temperature of the crucible wall and convective characteristics. Rate of evaporation of oxygen is governed by two mechanisms: i) convective transport of the oxygen from the bottom of the crucible and ii) carry over rate of the oxygen by argon flow outside the melt through gas-melt interface. In earlier

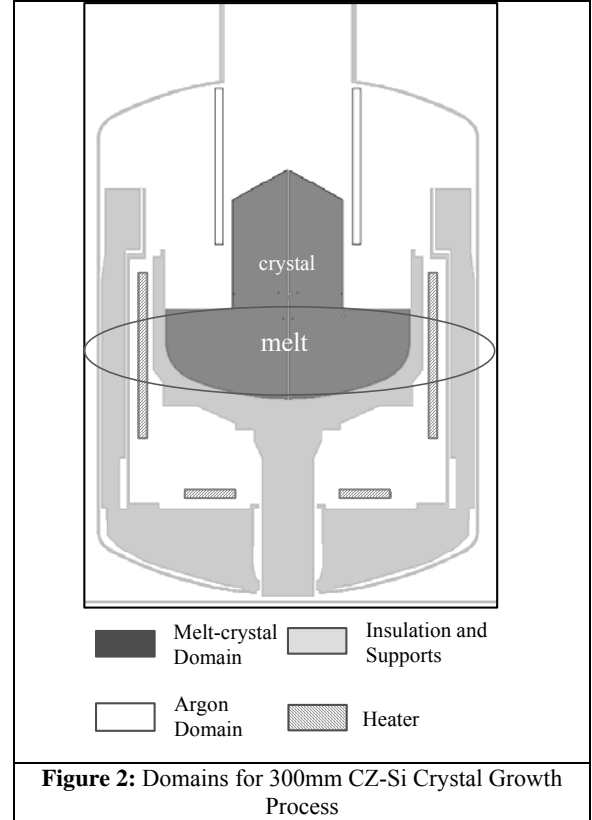
smaller size crucibles (Organ et al. 1987, Ramachandran et al. 1990 and Ma and Walker, 1997), boundary layer analysis enables accurate prediction of oxygen distribution due to laminar nature of flow. For large crystal growth processes (>200mm), flow is more unstable due to high Grashof (Gr) or Rayleigh (Ra) numbers ( $Gr \propto h^3$ ) (Zhang et al. 1999 and Grabner et al. 2000). Various previous studies (Kobayashi 1991, Kakimoto et al. 1996, Machida et al. 2000, Vizman et al. 2001, Watanabe et al. 2002) have indicated that the application of the external magnetic field is one of the effective ways to manipulate the flow characteristics and hence the oxygen. Interaction of thermo-fluidic flow with crystallization front is responsible for the non-uniformity of oxygen in the growing crystal. More than 99% of the oxygen evaporates through gas-liquid interface and evaporation is considered as instantaneous (Kobayashi et al. 1991, Togawa et al. 1995, Machida et al. 2000 and Smirnov and Kalaev, 2008). Hence accuracy in the flow prediction is indispensable. In the Cz crystal growth process, most of the heat from the heaters to the crucible is transferred by radiation. Various hardware internals such as surrounding insulations, crucible support and gas guide/heat shield above argon-melt interface affect the temperature and flow in the crucible. In order to understand the overall characteristics of the process, global analysis becomes an integral part of such study and such an approach has recently been used by several researchers for this purpose (Li et al. 2002, 2003, Kalaev et al. 2003, Liu et al. 2007, Smirnov and Kalaev, 2008).

This manuscript is organized in the following manner. Next section describes the model equations for Cz-Si process. This section goes through three subsections: model equations for Silicon melt flow, model equations for magneto-hydrodynamics, and transport equations for oxygen. Results are presented in the consecutive section, in which first melt flow and oxygen predictions are discussed in presence of crystal and crucible rotation conditions. Quantitative changes in oxygen distribution in the melt in presence of magnetic field (MR=0.64, 1 and 2.36) are reported the end of this section. Finally conclusions of this work are presented.

## MODEL DESCRIPTION

In this study, we have developed a global computational model to simulate the flow characteristics for various operating parameters. Different interconnected computational domains (shown in Figure 2) are considered in this model viz; melt-crystal (Si domain), argon (gas domain), graphite supports and surrounding insulation with outer steel wall (solid domain). Conduction, convection and radiation heat transport are considered in the fluid domains (melt and argon) and radiation and conduction heat transfer is considered in other solid regions. Solidification process is modeled using mushy zone approach in the melt/crystal domain. Details on furnace dimensions and flow model equations are provided in Gunjal et al. (2009). In this study, we further extend the applicability of this model to predict the oxygen distribution in the melt under various operating conditions including application of a magnetic field. The applied electromagnetic field produces currents in the conducting melt. In the presence of a magnetic field, current carrying melt fluid experiences a Lorentz force

that will alter the flow conditions of the melt. In this section, we provide the governing equations for melt flow in presence of a magnetic field and equations for electromagnetic fields and oxygen transport. Dimensional analysis of melt flow equations, parameters used in dimensioning the terms and the equations used for other domains, a reader should refer Gunjal et al. (2009) for more details.



### Governing Model Equations for Cz-Si process

#### Melt flow model equations

For an axi-symmetric domain, governing flow equations for melt flow in presence of applied electromagnetic field is given in dimensionless form as follows:

Continuity equation:

$$\frac{1}{r^*} \frac{\partial}{\partial r^*} (\rho r^* v_r^*) + \frac{R_c}{h_m} \frac{\partial}{\partial z^*} (\rho v_z^*) = 0 \quad (1)$$

r-component momentum balance:

$$v_r^* \frac{\partial v_r^*}{\partial r^*} - \left( \frac{Re_\theta}{Re_c} \right)^2 \frac{v_\theta^{*2}}{r^*} + v_z^* \frac{\partial v_r^*}{\partial z^*} = -\frac{\partial P^*}{\partial r^*} + \frac{1}{Re_c(1+1/\mu_t)} \left( \frac{\partial}{\partial r^*} \left( \frac{1}{r^*} \frac{\partial}{\partial r^*} (r^* v_r^*) \right) + \frac{1}{b^2} \frac{\partial^2 v_r^*}{\partial z^{*2}} \right) + NF_r^* \quad (2)$$

$\theta$ -component momentum balance:

$$v_r^* \frac{\partial v_\theta^*}{\partial r^*} + \frac{v_r^* v_\theta^*}{r^*} + v_z^* \frac{\partial v_\theta^*}{\partial z^*} = -\frac{1}{r^*} \frac{\partial P^*}{\partial \theta^*} + \frac{1}{Re_c(1+1/\mu_t)} \left( \frac{\partial}{\partial r^*} \left( \frac{1}{r^*} \frac{\partial}{\partial r^*} (r^* v_\theta^*) \right) + \frac{1}{b^2} \frac{\partial^2 v_\theta^*}{\partial z^{*2}} \right) + NF_\theta^* \quad (3)$$

z-component momentum balance:

$$v_r^* \frac{\partial v_z^*}{\partial r^*} + v_z^* \frac{\partial v_z^*}{\partial z^*} = -\frac{1}{b} \frac{\partial P^*}{\partial z^*} + \frac{1}{\text{Re}_c(1+1/\mu_t)} \left( \frac{1}{r^*} \frac{\partial}{\partial r^*} \left( r^* \frac{\partial v_z^*}{\partial r^*} \right) + \frac{1}{b^2} \frac{\partial^2 v_z^*}{\partial z^{*2}} \right) + \frac{Gr}{\text{Re}^2} T^* + NF_z^* \quad (4)$$

Energy balance equation:

$$v_r^* \frac{\partial T^*}{\partial r^*} + v_z^* \frac{\partial T^*}{\partial z^*} = \frac{1}{\text{PrRe}_c} \left( \frac{1}{r^*} \frac{\partial}{\partial r^*} \left( r^* \frac{\partial T^*}{\partial r^*} \right) + \frac{1}{b} \frac{\partial^2 T^*}{\partial z^{*2}} \right) + EcNj^{*2} \quad (5)$$

Dimensionless Number	Definition
Characteristic Reynolds number	$\text{Re}_c = \frac{\rho v_c R_c}{\mu}$
Rotational Reynolds Number	$\text{Re}_\Omega = \frac{\rho v_c R_c}{\mu}$
Grashoff number	$Gr = \frac{\beta g (T_c - T_m) R_c^3 \rho^2}{\mu^2}$
Prandtl number	$\text{Pr} = \frac{C_p \mu}{(k + k_t)}$
Eckert Number	$Ec = \frac{v_c^2}{C_p \Delta T}$
Interaction Parameter	$N = \frac{\sigma L B_o^2}{\rho v_c}$

**Table 1:** Different dimensionless groups involved in the above equations

#### Model for Electromagnetic Forces

For conducting Silicon material, in the presence of electromagnetic field, melt element experiences a force, *Lorentz force*, is calculated using electromagnetic field equations. These equations are described as follows:

Current produced in the Silicon melt is conservative, hence

$$\vec{\nabla} \cdot \vec{j}^* = 0 \quad (6)$$

Current density ( $j$ =in the moving fluid element is given by Ohm's law,

$$\vec{j}^* = \vec{E}^* + \vec{v}^* \times \vec{B}^* \quad (7)$$

Where  $E^*$  is defined as,

$$\vec{E}^* = \vec{E} / \sigma \vec{v}_c \vec{B}_o \quad (8)$$

$\vec{E}$  is the electric field which can be expressed in terms of electric potential ( $\phi$ ) as;

$$\vec{E} = -\vec{\nabla} \phi \quad (9)$$

From current density information and the applied magnetic flux density, Lorentz for acting on the fluid element is given as;

$$\vec{F}^* = (\vec{j}^* \times \vec{B}_o^*) \quad (10)$$

Therefore, components of the Lorentz force used in the above momentum balance equations are as follows:

$$F_r^* = E_r^* + (j_\theta^* B_z^*) \quad (11)$$

$\theta$ -component:

$$F_\theta^* = E_\theta^* + (j_z^* B_r^* - j_r^* B_z^*) \quad (12)$$

z-component:

$$F_z^* = E_z^* + (j_\theta^* B_r^*) \quad (13)$$

Boundary conditions are required for the solution of the electric potential equation. Boundaries of the crucible wall, crystal walls in contact with argon gas and Silicon melt-gas interface are considered as an insulated. Crystal's conductivity is very small as compared to the conductivity of the Silicon melt. Previous researchers have used the crystal-melt interface as an insulation (neglecting the electric conductivity of crystal) or current continuity at the melt-crystal interface. In this study, we treat crystal as an insulator with small electric current passes through the crystal. Crucible is rotating and is considered as insulator; therefore following condition is valid at the walls of the crucible:

$$n \cdot (\vec{v} \times \vec{B}_o) = 0 \quad (14)$$

where, components of the velocity vector  $v_r$  and  $v_\theta$  for the crucible are zero and crucible is rotating at a constant angular velocity.

#### Transport Equations for Oxygen

Governing equation for the transport of oxygen in the Silicon melt is considered as transportation of inert dilute species and hence presented in the form of convection-diffusion equation as follows:

$$\vec{\nabla} \cdot (\rho \vec{v} C_o) = \vec{\nabla} \cdot (D_{\text{eff}} \vec{\nabla} C_o) \quad (15)$$

where  $D_{\text{eff}}$  is the effective diffusivity of the oxygen defined as:

$$D_{\text{eff}} = \frac{\mu}{Sc} + \frac{\mu}{Sc_t} \quad (16)$$

Where  $Sc = 10$  and  $Sc_t = 0.9$

#### Boundary conditions for the oxygen transport

At crucible wall, dissolution of the silica crucible is occurred by following reaction,



Oxygen dissolution rate is measured by Huang et al. (1994) is given as:

$$C_o(T) = 1.32 \times 10^{19} \exp\left(\frac{-3.20 \times 10^3}{T}\right) \quad (18)$$

At melt-crystal interface, segregation coefficient for oxygen is assumed to be one. For lower pull rate and diffusivity in the solids, following boundary condition is valid (normal gradient is zero):

$$\frac{\partial C_o}{\partial n} = 0 \quad (19)$$

At the gas-melt interface, evaporation of the oxygen is considered using following rate equation (Togawa et al. 1995):

$$D \frac{\partial C_o}{\partial n} = \varepsilon(T) C_o \quad (20)$$

$$\varepsilon(T) = 5.9152 \times 10^7 \exp\left(\frac{-4.1559 \times 10^4}{T}\right) \quad (21)$$

Silicon
<i>Melt Properties</i>
Density = 2530 kg/m <sup>3</sup>
Viscosity = 0.0007 Pa.s
K (Silicon melt) = 64 W/mK
Cp = 1000 J/kg K
Coefficient of Thermal Expansion ( $\beta$ ) = 0.000141,
Thermo-capillary Coefficient = -0.00036 N/mK.
<i>Crystal Properties</i>
Density = 2500 kg/m <sup>3</sup>
K = 22 W/mK at 1683 K & $f(T)$ .
Cp = 1000 J/kg K
$\varepsilon = 0.8$
Melting Temperature = 1683K,
Heat of Solidification = 1410000J/kg
Oxygen
Diffusivity = $3 \times 10^{-8}$ m <sup>2</sup> /sec
Segregation Co-efficient for Oxygen = 1

**Table 1:** Properties of Materials Used in Model

Model equations and corresponding boundary conditions of electromagnetic fields and oxygen transport are implemented in previously developed model for flow predictions in 300mm Cz process (Gunjal et al. 2009) through User Defined Functions (UDFs) in the Fluent 6.3.26 code and simulation results are discussed in the following section.

## RESULTS

In the following sections, we discuss the numerical results on the melt flow simulations to demonstrate the implications of local flow variation on oxygen distribution in the melt. We present results for various case studies: in the first case, melt flow under crystal and crucible rotation condition is considered and oxygen distribution in the melt is predicted. In the subsequent cases, application of external CUSP magnetic field with magnetic ratio MR=0.64, 1 and 2.38 are considered for simulations. Effect of these operating parameters on oxygen distribution is discussed with the help of simulation results.

### Melt under rotation conditions

Co-rotation of the crystal and crucible is considered and the results of predicted flow profile and temperature distribution is shown in the Figure 3a-b. Centrifugal force due to the crystal rotation strengthens the counter-rotating flow cell in the central region of the crucible (call Taylor-Proudman cell). Near the crucible edge, buoyancy driven flow cell is observed which occupies entire crucible region in absence of any rotations. Rotation facilitates decrease in meridional flow considerably and hence reduces adverse effects of turmoils produces by thermal flows. Due to reduced meridional flow, conductive heat transfer becomes comparable with convection in the outer region of the crucible (for more details, ref. Gunjal et al. 2009). Here, it is important to study oxygen distribution in such complex flow system.

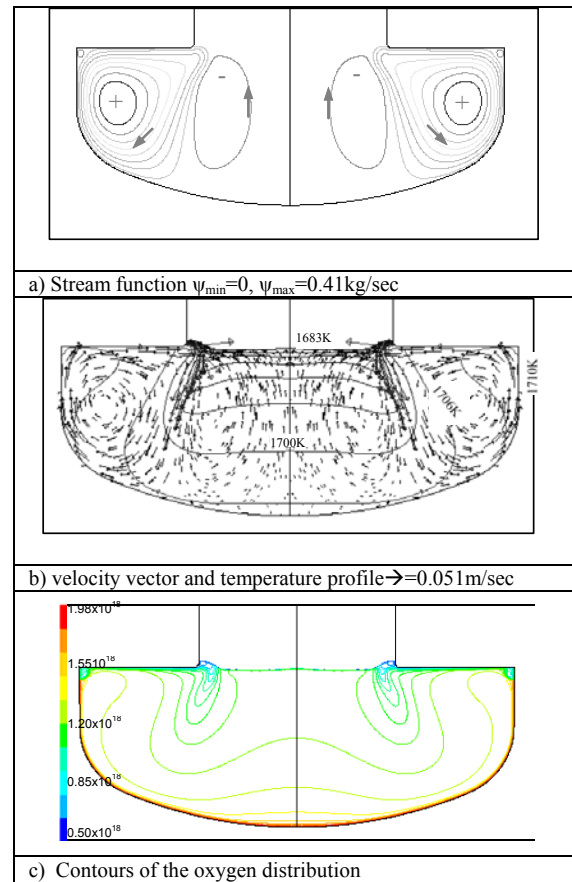


**Figure 3:** Simulation results for rotating crystal (12rpm) and crucible (1.5rpm)

Flow structure in the crucible indicates that oxygen dissolved from the crucible wall is carried away by meridional flow either towards gas-melt interface (transported by buoyancy flow cell) or towards crystallization front (transported by Taylor-Proudman cell). Therefore, oxygen carried by centrifugal flow cell get incorporated into the crystal, however near the edge of the crystal, the buoyancy cell is interacting with the crystal. Most of the oxygen carried by the buoyancy cell evaporates through gas-melt interface and the remaining is carried towards crystallization front. The portion of the crystal in contact with buoyancy cell receives less oxygen from melt compared to the central portion of the crystal. Hence, oxygen level in the core region of the crucible is higher  $1.4 \times 10^{18}$  atoms/cm<sup>3</sup> compared to edge region  $> 1 \times 10^{18}$  atoms/cm<sup>3</sup>.

## Effect of External Magnetic Field

### CUSP magnetic field configurations

CUSP magnetic field can be produced by using two coils in the upper and lower portion of the system. The magnitude and direction of the external magnetic field can be varied by changing the current and the ratio of currents in the upper and the lower coil respectively. CUSP magnetic field ratio (MR) is the ratio of the current in the lower to the upper coil. For example, MR=1 indicates same current in both coils and field generated under these conditions produces zero gauss plane at the centre of the melt-crystal interface as shown in Figure 4b. MR=0.64 indicates more current in the lower coil and zero gauss plane lie inside the crystal (Figure 4a), while MR=2.38 indicates zero gauss plane lie inside the melt as shown in Figure 4c.

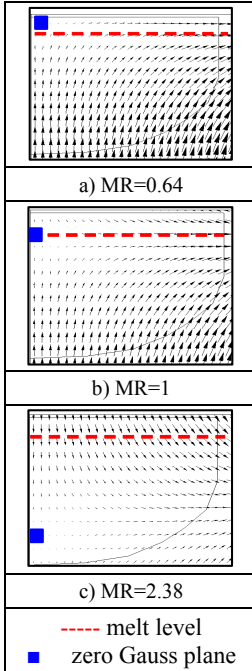


**Figure 4:** CUSP field configurations

### Melt flow in presence of magnetic field

For simulating flow in presence of the magnetic field, crystal rotation 12 rpm and crucible rotation 1.5 rpm is considered as a base case. Predicted flow and temperature profiles in presence of CUSP magnetic field for MR=0.64 are shown in Figure 5a Figure 6a. Application of external magnetic field show two major changes in the melt flow; strength of the magnetic field is higher in the core and the edge region of the crucible, which diminishes the effect of crucible rotation. Strength of magnetic field is lower near the crystallization front; hence crystal rotation effect produces strong centrifugal flow below the crystal (ref. Figure 5a and Figure 6a). This flow carries heat from the bottom of the crucible and produces high temperature gradients near the crystallization front. This heat also facilitates movement of melt-crystal interface inside the crystal (not shown here, note that the temperature gradients and interface position are the important parameters for the defects and dislocations studies).

For MR=1, zero Gauss plane is located at the centre of crystal-melt interface, the region of negligible magnetic strength. Near the edge of the crucible, magnetic field strength is lower compare to above case. Decrease in magnetic field strength enhances the buoyancy driven flow slightly (see Figure 5b and Figure 6b). Since magnetic field strength is negligible at the centre, crystal pumping effect strengthens the Taylor-Prudman cell under the crystal. Flow pattern for both cases (MR=0.64 and 1) are similar in nature, except stronger meridional flow cells

in later case. Therefore, it is interesting to see change in oxygen concentration due to marginal change in flow

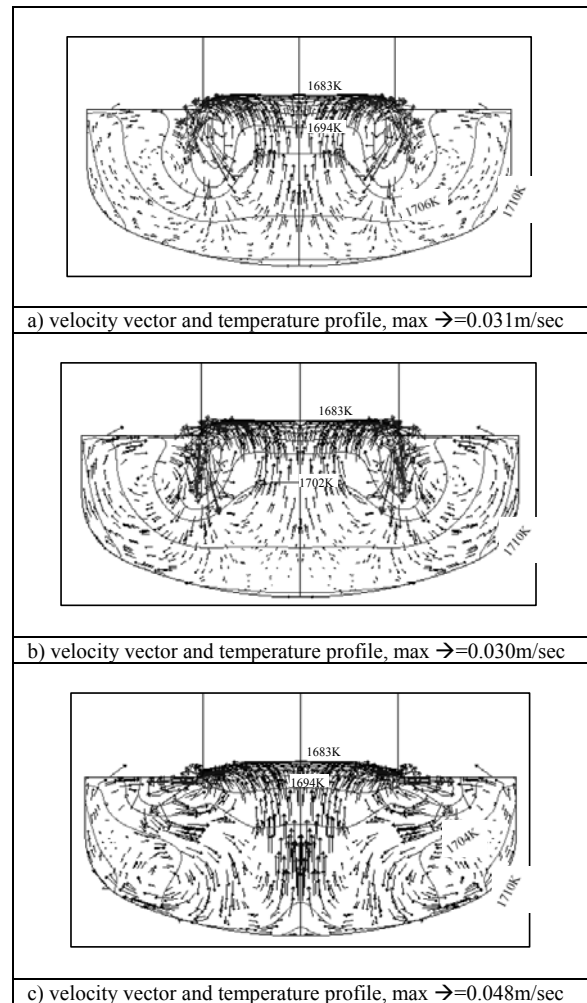


**Figure 5:** Velocity vectors and temperature contours

For MR=2.38, magnetic field lines are opposite to that of MR=1 case with zero Gauss plane at the bottom of the crucible. Predicted flow profiles are considerably different from previous two cases (ref. Figure 5c and Figure 6 c). Field lines are stronger in the upper portion of the crucible and weaker at the bottom of the crucible. Simulation results show that meridional flow in the outer portion of the crucible is damped because of applied magnetic field, which results into expansion of flow cell produced by centrifugal action due to crystal rotation. Model results show (ref. Figure 5c and Figure 6c), centrifugal cell occupies most part of the crucible. Lower strength of the magnetic field near the bottom of the crucible also enhances the buoyancy driven flow to some extent. Therefore, buoyancy driven flow remain dominant near the crucible edge region and centrifugal flow cell in the crystallization front. Implications of this changed flow profiles on variation of oxygen in the melt is discussed in the following section.

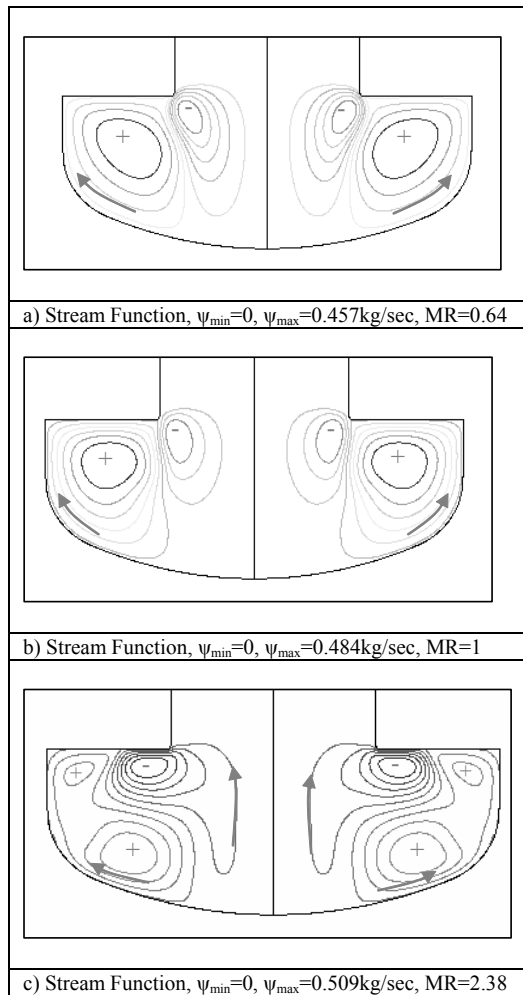


**Figure 6:** Predicted stream functions for various MR

### Oxygen Distribution in the Melt

In the presence of a magnetic field, two changes in the melt flow are observed: azimuthal flow due to crucible rotation gets suppressed and counter rotating buoyancy cell increases to some extent compared to the co-rotating centrifugal cell underneath the crystal (Ref. Figure 5 and Figure 6). Variation of oxygen concentration in the melt, hence in the crystal, is the function of the relative strength of these flow cells. Buoyancy driven cell in the outer region of the crucible carries dissolved oxygen towards the gas-melt interface and central co-rotating centrifugal cell present below the crystal carries dissolved oxygen towards the crystallization front. Simulation results indicate that the relative strength of the central centrifugal cell is higher when magnetic field ratio is increased or decreased from MR=1 and this trend is more pronounced for MR=2.38. Therefore, oxygen concentration is higher in the central region for MR=0.64 and 2.38 (ref. Figure 7). Most of the oxygen reaches to the gas-melt interface through buoyancy driven cell. However, for MR=2.38, only part of the oxygen carried from the crucible wall reaches to the gas-melt interface through external buoyancy driven flow. Oxygen evaporation rate is lower due to extended centrifugal cell in the core region of the crucible. Therefore, at MR=2.36, oxygen concentration in

the melt is higher than other two cases. For MR=1, both flow cells are marginally stronger than the case with MR=0.64. Crucible wall temperature is more or less same for these cases; hence oxygen concentration in the melt is function of the dissolution rate at the walls and evaporation rate at the gas-melt interface. Higher buoyancy flow results in lower oxygen concentration in the melt, indicating instantaneous evaporation is playing substantial role in deciding oxygen concentration levels in the melt.

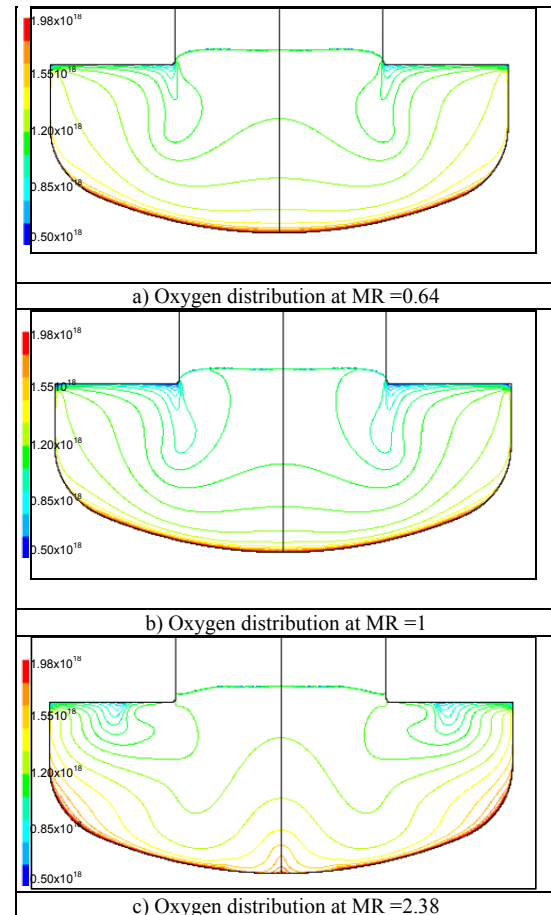


**Figure 7:** Oxygen concentration contours in the melt domain

Oxygen concentration at the crystallization front is compared with and without field case in Figure 8. Centrifugal flow cell for without magnetic field case is weaker than with magnetic field cases. Oxygen depleted buoyancy driven flow penetrates into the edge of the crystal and hence higher radial non-uniformity is observed near the crystallization front without the magnetic field. Such stratification quantitatively is shown in Figure 8. Oxygen concentration falls below  $1 \times 10^{18} \text{atom/cm}^3$  near the edge of the crystal and as high as  $1.15 \times 10^{18} \text{atoms/cm}^3$  in the central region of the crystal. Applied magnetic field prevents oxygen depleted buoyancy driven flow interaction with the crystal edge and hence oxygen is uniformly distributed near the crystal-melt interface. As discussed earlier, higher oxygen concentration is also observed near crystallization front for MR=2.36 and 0.64 due to centrifugal and buoyancy cell respectively.

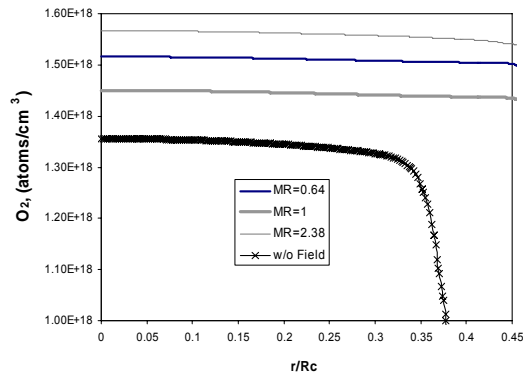


**Figure 8:** Oxygen distribution near the crystallization front

## CONCLUSIONS

A global model results for the industrial Cz-Si process are presented to demonstrate the effect of local melt flow behavior on oxygen concentration in the melt. Our results suggest that local variation of the flow cells inside the crucible has a significant impact on dissolution rate and evaporation rate. The crystal and crucible rotation stabilizes the flow generated by thermo-fluids and also decrease the dissolution rate of oxygen in the melt. Melt flow simulation results under different CUSP magnetic field configurations indicate that the increase in centrifugal pumping of melt underneath the crystal brings the interface position inside the crystal. High melt flow near the edge of the crucible prevents the interaction of the oxygen depleted buoyancy cell. Hence oxygen concentration is more homogeneous at the crystallization front as compare to the cases without magnetic field. Model results presented are found to be helpful for getting insight into the complex flow behaviour of melt in Cz process and devising operating guidelines for Cz process.

## ACKNOWLEDGEMENT

We are thankful to MEMC for providing financial support for this work and to Dr. Milind S. Kulkarni for his valuable inputs during this work. We are also thankful for Mr. Harold Korb for his guidance to calculating static fields for this system.

## REFERENCES

- GRABNER, O., MUHE, A., MULLER, G., TOMZIG, E., VIRBULIS, J., and VON AMMON W., (2000), *Materials Science and Engineering*, **B73**, 130–133.
- GUNJAL P. R., KULKARNI M. S. and RAMACHANDRAN P. A., (2009), “Effect of crystal and crucible co-rotations on melt flow in 300mm Cz-Si process using multi-domain global CFD model”, *Journal of Crystal Growth*, under review.
- HUANG X.M., TERASHIMA K., SASAKI H., TOKIZAKI E., ANZAI Y., KIMURA S., (1994), *Japanese Journal of Applied Physics*, **33**, 1717.
- KAKIMOTO K., YI K. and EGUCHI M., (1996), “Oxygen transfer during single Silicon crystal growth in Czochralski system with vertical magnetic fields”, *Journal of Crystal Growth*, **163**(3), 238-242.

KALAEV V.V., YU., I., EVSTRATOV, YU. N. and MAKAROV, (2003), “Gas flow effect on global heat transport and melt convection in Czochralski Silicon growth”, *Journal of Crystal Growth*, **249**, 87–99.

KOBAYASHI N., (1991), “Oxygen transport under an axial magnetic field in Czochralski Silicon growth”, *Journal of Crystal Growth*, **108**(1-2), 240-246.

LI MINGWEI, LI Y., IMAISHI N. and TSUKADA T., (2002), “Global simulation of a Silicon Czochralski furnace”, *Journal of Crystal Growth*, **234**, 32–46.

LIU L., NAKANO S. and KAKIMOTO K., (2007), “Investigation of oxygen distribution in electromagnetic CZ–Si melts with a transverse magnetic field using 3D global modelling”, *Journal of Crystal Growth*, **299**, 48–58.

MA N. and WALKER J.S., (1997), “Validation of strong magnetic field asymptotic models for dopant transport during semiconductor crystal growth”, *Journal of Crystal Growth*, **180**, 401-409.

MACHIDA N., HOSHIKAWA K. and SHIMIZU Y., (2000), “The effects of argon gas flow rate and furnace pressure on oxygen concentration in Czochralski Silicon single crystals grown in a transverse magnetic field”, *Journal of Crystal Growth*, **210**(4), 532-540.

ORGAN E. and RILEY N., (1987), “Oxygen transport in magnetic Czochralski growth of Silicon”, *Journal of Crystal Growth*, **82**(3), 465-476.

RAMACHANDRAN P. A., M. P. DUDUKOVIC and DORSEY D., (1990), “Modeling the effect of operating parameters on oxygen content in Czochralski growth of Silicon”, *Journal Electrochemical Society*, **137**, 10.

SMIRNOV A.D. and KALAEV V.V., (2008), “Development of oxygen transport model in Czochralski growth of Silicon crystals”, *Journal of Crystal Growth* **310**(12), 1, 2970-2976.

TOGAWA S., X. HUANG, K. IZUNOME, K. TERASHIMA and KIMURA S. (1995), “Oxygen transport analysis in Czochralski Silicon melt by considering the oxygen evaporation from the melt surface”, *Journal of Crystal Growth*, **148**(1-2), 70-78.

ZHANG T., G. -X. WANG, H. ZHANG, F. LADEINDE and PRASAD V., (1999), “Turbulent transport of oxygen in the Czochralski growth of large Silicon crystals”, *Journal of Crystal Growth*, **198-199**, 141-146.